

# Tube-RRT\*: Efficient Homotopic Path Planning for Swarm Robotics Passing-Through Large-Scale Obstacle Environments

Pengda Mao<sup>1</sup>, Shuli Lv<sup>1</sup>, and Quan Quan<sup>1</sup>

**Abstract**—Recently, the concept of optimal virtual tube has emerged as a novel solution to the challenging task of navigating obstacle-dense environments for swarm robotics, offering a wide ranging of applications. However, it lacks an efficient homotopic path planning method in obstacle-dense environments. This paper introduces Tube-RRT\*, an innovative homotopic path planning method that builds upon and improves the Rapidly-exploring Random Tree (RRT) algorithm. Tube-RRT\* is specifically designed to generate homotopic paths for the trajectories in the virtual tube, strategically considering opening volume and tube length to mitigate swarm congestion and ensure agile navigation. Through comprehensive comparative simulations conducted within complex, large-scale obstacle environments, we demonstrate the effectiveness of Tube-RRT\*.

## I. INTRODUCTION

In recent years, swarm robotics has emerged as a promising application in various fields, including search and rescue operations, environmental monitoring, agriculture, exploration, and logistics. A current focus is on determining the safe, reliable, and smooth movement of swarm robotics within large-scale obstacle environments.

In addressing the issue of robot swarms passing through large-scale obstacle environments, there are currently numerous methods available, including trajectory planning [1], control-based methods [2], and virtual tube approaches [3]. The method of swarm trajectory planning employs a hierarchical structure, which enables the smooth movement of the swarm. However, when the number of robots is large and the environment is complex, the optimization problems of the trajectory planning become intricate and difficult to solve, leading to high computational load and frequent replanning [4], [5]. Control-based methods, on the other hand, provide instructions for the current moment based on the states of surrounding agents, which have stability, simplicity, and low computation cost. However, they lack prediction and the simplicity of robot modeling leads to less smooth movement and susceptibility to local minima. Therefore, by combining the strengths of these two methods, the optimal virtual tube method proposed in our previous work [6] is a method suitable for large-scale swarm movement. It confines the robot swarm in free space and achieves low computation cost to pass through obstacle environments through centralized trajectory planning and distributed control.

Optimal virtual tube planning is one of the homotopic trajectory planning methods [7] aiming at providing an infinite

set of homotopic optimal trajectories for robotic swarm to swiftly and smoothly pass through obstacle environments as a group. Therefore, the optimal virtual tube needs the homotopic path planning as the front end of the trajectory planning and seeks to minimize the contraction of the tube volume to prevent swarm congestion.

The path planning methods are divided into several categories such as graph-based methods [8] and sample-based methods [9] which are mostly used in applications. On the one hand, the graph-based method designs a rule to find an optimal path for each robot in a graph. There are many widely used algorithms including Dijkstra [10], Greedy best first search [11], and A\* [12], while computation cost grows exponentially with the dimensions and resolution of the map. Sample-based methods for path planning effectively construct a free space graph in configuration space by using random samples as nodes and connecting nearby samples. These methods excel in high-dimensional spaces and are divided into multi-query and single-query approaches. Multi-query methods, such as the Probabilistic Random Map (PRM) [13], build a graph and query for feasible paths between start and goal points. Variants like PRM\* are asymptotically optimal, meaning they can find the optimal path as the number of samples approaches infinity. Single-query methods, tailored for online path planning, include Rapidly-exploring Random Trees (RRT) [14] which grows a tree with probabilistic completeness towards finding a feasible path. The RRT\* algorithm [15], a modification of RRT, has been proven asymptotically optimal, and subsequent works [16], [17], [18] have adapted RRT\* for diverse environments.

Homotopic paths in topology [19] refers to a concept that illustrates the continuous deformation between two paths. In other words, two paths are homotopic in configuration space if one can be continuously deformed into the other in free space without breaking the continuity. There are many works on finding homotopic paths to speed up the computation. A reference frame determining the topological relationship between obstacles is used to compute a topological graph for restriction criteria of homotopy classes [20]. Both the Homotopic RRT (HRRT) [21] and the Homotopic A\* (HA\*) [12] explore the direction in complex space by checking the intersections with the reference frame to generate the homotopic paths. However, these homotopic path planning methods focus on accelerating the computation speed of a single robot to find a single optimal path [22], [23]. Even in swarm path planning problem, due to the lack of coordination among agents in the swarm, the planning of homotopic paths is limited to a single robot exploring a collision-avoidance

<sup>1</sup>Pengda Mao, Shuli Lv, and Quan Quan are with School of Automation Science and Electrical Engineering, Beihang University, Beijing, 100191, P.R. China (e-mail: maopengda@buaa.edu.cn; lvshuli@buaa.edu.cn; qq\_buaa@buaa.edu.cn).

path of a specific shape, such as an elliptical homotopy path [24], which can not be applied in the optimal virtual tube planning and has high computation cost.

In our previous work, we generated homotopic paths by repeatedly applying the RRT\* algorithm [15] in a simply connected free space, a method that is time-consuming and tends to traverse narrow gaps in search of the shortest path. This leads to sudden contractions in the volume of the generated virtual tube, causing congestion within the swarm. Thus, in this paper, we propose a novel infinite homotopic path planning algorithm for the optimal virtual tube based on the RRT\* algorithm, named Tube-RRT\*. The main contributions of this paper are as follows:

- An efficient homotopic path planning algorithm, named Tube-RRT\*, is proposed for optimal virtual tube planning. Considering both the path length and the volume of openings, the homotopic paths found by Tube-RRT\* algorithm pass through large openings, which are suitable for constructing the virtual tube.
- A novel centralized homotopic path planning method plans infinite homotopic paths centrally with the computation complexity  $O(n(\log n + 1) + 1)$ . Compared with computation complexity  $O(n(\log n + 1))$  of the RRT\* for a single robot, the proposed algorithm is efficient for swarm robotics.
- A proof demonstrates that the proposed algorithm tends to find homotopic paths maintaining the smallest number of path points and equal volumes of cross-sections if the total volume and the length of virtual tube are fixed.
- The effectiveness of the proposed algorithm for optimal virtual tube planning is validated through various comparisons in simulations.

## II. PRELIMINARIES AND PROBLEM FORMULATION

In this section, we first introduce the related concepts of the optimal virtual tube and homotopic paths. Then, a specific homotopic path planning problem is described.

### A. Preliminaries

*Definition 1 (Virtual Tube [6]):* A virtual tube  $\mathcal{T}$ , as shown in Fig. 1(a), is a set in a configuration space  $X$  represented by a 4-tuple  $(\mathcal{C}_0, \mathcal{C}_1, \mathbf{f}, \mathbf{h})$  where

- $\mathcal{C}_0, \mathcal{C}_1$ , called *terminals*, are disjoint bounded convex subsets in  $n$ -dimension space.
- $\mathbf{f}$  is a *diffeomorphism*:  $\mathcal{C}_0 \rightarrow \mathcal{C}_1$ , so that there is a set of order pairs  $\mathcal{P} = \{(\mathbf{q}_0, \mathbf{q}_m) \mid \mathbf{q}_0 \in \mathcal{C}_0, \mathbf{q}_m = \mathbf{f}(\mathbf{q}_0) \in \mathcal{C}_1\}$ .
- $\mathbf{h}$  is a smooth<sup>1</sup> map:  $\mathcal{P} \times \mathcal{I} \rightarrow \mathcal{T}$  where  $\mathcal{I} = [0, 1]$ , such that  $\mathcal{T} = \{\mathbf{h}((\mathbf{q}_0, \mathbf{q}_m), t) \mid (\mathbf{q}_0, \mathbf{q}_m) \in \mathcal{P}, t \in \mathcal{I}\}$ ,  $\mathbf{h}((\mathbf{q}_0, \mathbf{q}_m), 0) = \mathbf{q}_0$ ,  $\mathbf{h}((\mathbf{q}_0, \mathbf{q}_m), 1) = \mathbf{q}_m$ . The function  $\mathbf{h}((\mathbf{q}_0, \mathbf{q}_m), t)$  is called a *trajectory* for an order pair  $(\mathbf{q}_0, \mathbf{q}_m)$ .

<sup>1</sup>A real-valued function is said to be smooth if its derivatives of all orders exist and are continuous.

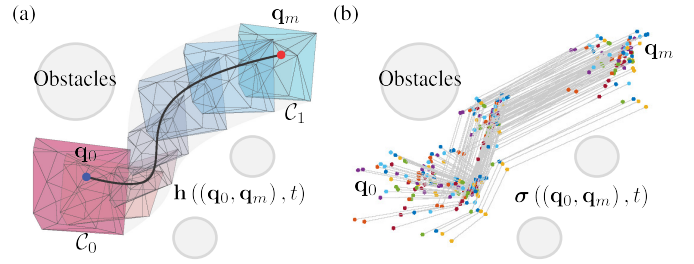


Fig. 1. Virtual tube in obstacle environments. (a) The purple and blue polyhedrons are terminals. The black curve is the trajectory from  $\mathbf{q}_0 \in \mathcal{C}_0$  to  $\mathbf{q}_m \in \mathcal{C}_1$ . (b) The colorful points denote path points of the homotopic paths and the gray lines represent homotopic paths  $\sigma((\mathbf{q}_0, \mathbf{q}_m), t)$ .

Intuitively, the optimal virtual tube is a set of infinite optimal trajectories. The mathematical definition is as follows:

*Definition 2 (Optimal Virtual Tube [6]):* A virtual tube  $\mathcal{T}$  is *optimal* with respect to a cost  $g$  if every trajectory in the tube is *optimal* with respect to a cost  $g$ , namely  $\mathcal{T} = (\mathcal{C}_0, \mathcal{C}_1, \mathbf{f}, \mathbf{h}^*)$ .

*Definition 3 (Path):* For any order pair  $(\mathbf{q}_0, \mathbf{q}_m) \in \mathcal{P}$ , the *path* is a continuous function  $\sigma((\mathbf{q}_0, \mathbf{q}_m), t) : \mathcal{P} \times \mathcal{I} \rightarrow X$  where  $\sigma((\mathbf{q}_0, \mathbf{q}_m), 0) = \mathbf{q}_0$  and  $\sigma((\mathbf{q}_0, \mathbf{q}_m), 1) = \mathbf{q}_m$ ,  $m$  represents the number of the path points. And, the paths  $\sigma((\mathbf{q}_{0,k}, \mathbf{q}_{m,k}), t)$  is the boundary paths if the points  $\mathbf{q}_{0,k}$  and  $\mathbf{q}_{m,k}$  are the vertexes of the terminals  $\mathcal{C}_0$  and  $\mathcal{C}_1$  respectively.

*Definition 4 (Homotopic Paths):* For any  $\sigma_1, \sigma_2 \in \Sigma_\sigma$ , the paths  $\sigma$  in the set  $\Sigma_\sigma$ , as shown in Fig. 1(b), are called *homotopic paths* if there is a continuous map  $\mathbf{H} : \mathcal{I} \times \mathcal{I} \rightarrow X$  such that  $\mathbf{H}(t, 0) = \sigma_1((\mathbf{q}_{0,1}, \mathbf{q}_{m,1}), t)$ ,  $\mathbf{H}(t, 1) = \sigma_2((\mathbf{q}_{0,2}, \mathbf{q}_{m,2}), t)$ ,  $\mathbf{H}(0, 0) = \mathbf{q}_{0,1}$ ,  $\mathbf{H}(1, 0) = \mathbf{q}_{m,1}$ ,  $\mathbf{H}(0, 1) = \mathbf{q}_{0,2}$ ,  $\mathbf{H}(1, 1) = \mathbf{q}_{m,2}$ .

It should be noted that the definition of homotopic paths in *Definition 4* is a generalization of those defined in other works [7], [24], without fixed start and goal points to accommodate the requirements of virtual tube planning.

*Definition 5 (Tube Path Length):* The tube path length of the virtual tube  $\mathcal{T} = (\mathcal{C}_0, \mathcal{C}_1, \mathbf{f}, \mathbf{h})$  is the average length of the center path  $\sigma_o$  in the virtual tube, which is expressed as  $L_{\mathcal{T}}(\sigma_o)$ . The center paths  $\sigma_o$  is linear combination of the boundary paths  $\sigma_k$ , which is expressed as

$$\sigma_o = M^{-1} \sum_{i=1}^M \sigma_i, \sigma_i \in \sigma, \quad (1)$$

where  $M$  is the number of the boundary paths.

### B. Homotopic Path Planning Problem Formulation

This work aims to develop a method to determine homotopic paths for the optimal virtual tube in 3-D space, considering both the tube path length and the opening volume. The problem is described as follows:

Let  $X \in \mathbb{R}^3$  be the configuration space,  $X_{\text{obs}}$  be the obstacle space. Thus, the free space is denoted as  $X_{\text{free}} = X/X_{\text{obs}}$ . The homotopic path planning algorithm aims to determine the homotopic paths  $\sigma^*((\mathbf{q}_0, \mathbf{q}_m), t) \in X_{\text{free}}$  such that

$$\sigma^* = \arg \min_{\sigma} f_1(\sigma) + f_2(\sigma), \quad (2)$$

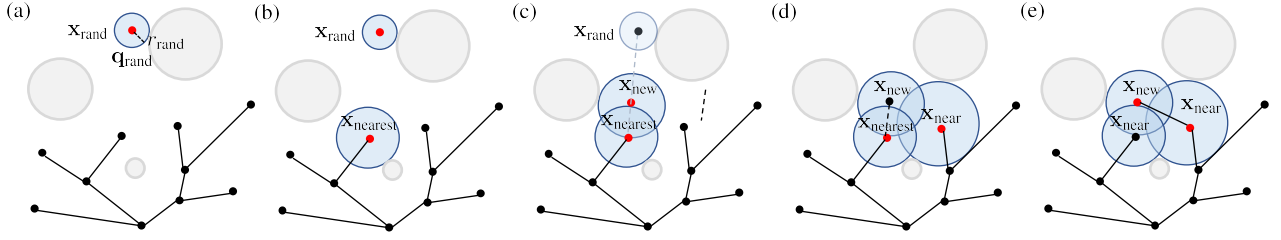


Fig. 2. The scheme of Tube-RRT\* algorithm. Gray circles are obstacles and blue circles are centered in the red and black points. (a) Step 1: Sample a sphere  $\mathbf{x}_{\text{rand}}$  which is denoted by the blue circle centered in  $\mathbf{q}_{\text{rand}}$  with radius  $r_{\text{rand}}$  in free space. (b) Step 2: Find the nearest sphere  $\mathbf{x}_{\text{nearest}}$  in the tree. (c) Step 3: Steer the sample sphere  $\mathbf{x}_{\text{rand}}$  towards the nearest sphere  $\mathbf{x}_{\text{nearest}}$  to obtain  $\mathbf{x}_{\text{new}}$  which has an intersection with  $\mathbf{x}_{\text{nearest}}$ . (d) Step 4: Find all the spheres in the tree which have intersections with the  $\mathbf{x}_{\text{new}}$  to obtain the set  $X_{\text{near}}$ . (e) Step 5: Rewire the sphere  $\mathbf{x}_{\text{new}}$  to a sphere in the tree to approach the minimum cost. And the spheres in  $X_{\text{near}}$  also are rewired.

where  $f_1, f_2 : X \rightarrow \mathbb{R}_{\geq 0}$  are functions related to tube path length and volume respectively.

### III. METHODS

In this section, a new modified RRT\* algorithm, Tube-RRT\*, is introduced. First, this new homotopic path planning algorithm is outlined in *Algorithm 1*. Subsequently, some primitive procedures are defined. Finally, the analysis of properties of the proposed algorithm is presented.

#### A. Outline

The proposed algorithm shown in *Algorithm 1* is divided into 6 steps. Step 1 (line 5-7, Fig. 2(a)): Sample a random sphere  $\mathbf{x}_{\text{rand}}$  centered in  $\mathbf{q}_{\text{rand}}$  with the radius  $r_{\text{rand}}$  which is the minimum distance to obstacles in free space, so that the sphere  $\mathbf{x}_{\text{rand}}$  is denoted as  $\mathbf{x}_{\text{rand}} = (\mathbf{q}_{\text{rand}}, r_{\text{rand}})$ . Step 2 (line 8, Fig. 2(b)): Find the nearest sphere  $\mathbf{x}_{\text{nearest}}$  to the random sphere  $\mathbf{x}_{\text{rand}}$  in the tree  $\mathcal{G}$ . Step 3 (line 9-10, Fig. 2(c)): Steer the random sphere  $\mathbf{x}_{\text{rand}}$  towards the nearest sphere  $\mathbf{x}_{\text{nearest}}$  to obtain a new sphere  $\mathbf{x}_{\text{new}}$  which has an intersection between  $\mathbf{x}_{\text{nearest}}$  and  $\mathbf{x}_{\text{new}}$ . Meanwhile, the radius  $r_{\text{new}}$  of  $\mathbf{x}_{\text{new}}$  remains consistent with the distance to obstacles, that is constantly changing and restricted by the minimum radius  $r_{\text{min}}$ . Step 4 (line 11, Fig. 2(d)): Find a set  $X_{\text{near}}$  that contains all spheres intersected with the new sphere  $\mathbf{x}_{\text{new}}$  in the tree  $\mathcal{G}$ . Step 5 (line 12-13, Fig. 2(e)): Rewire the tree to choose the connections among  $\mathbf{x}_{\text{new}}$  and the spheres in the set  $X_{\text{near}}$  with the minimum cost.

#### B. Proposed Algorithm

The Tube-RRT\* is a modified version of the RRT\* algorithm, which modifies functions of steering, finding near nodes, and rewiring to consider both the volumes of sphere-sphere intersections and the tube path length in samples. Before the discussion and analysis, the functions in the proposed algorithm are detailed in the following.

**ObstacleFree:** Connect two centers in spheres to obtain a line segment. Check if there is any intersection between the obstacles and this line segment. If an intersection is detected, return false; otherwise, proceed with true.

**FindMaxRadius:** Find the nearest obstacle point  $\mathbf{q}_{\text{obs}}$  to the input point  $\mathbf{q}$ . Subsequently, the minimum distance  $r$  between  $\mathbf{q}_{\text{obs}}$  and  $\mathbf{q}$  is designated as the radius of a sphere centered at point  $\mathbf{q}$ , ensuring the sphere  $\mathbf{x} = (\mathbf{q}, r)$  remains within the free space. Moreover, the radius  $r$  must be less

---

#### Algorithm 1 Tube-RRT\*

---

**Input:** start point  $\mathbf{q}_{\text{init}}$ , goal point  $\mathbf{q}_{\text{goal}}$ , space  $\mathcal{X}$

**Output:**  $\mathcal{G} = (V, E)$

```

1:  $r_{\text{init}} \leftarrow \text{FindMaxRadius}(\mathbf{q}_{\text{init}})$ ;
2:  $\mathbf{x}_{\text{init}} \leftarrow (\mathbf{q}_{\text{init}}, r_{\text{init}})$ ;
3:  $V \leftarrow \{\mathbf{x}_{\text{init}}\}$ ;  $E \leftarrow \emptyset$ ;  $\mathcal{G} = (V, E)$ ;
4: for  $i = 1, \dots, n$  do
5:    $\mathbf{q}_{\text{rand}} \leftarrow \text{SampleFree}_i$ ;
6:    $r_{\text{rand}} \leftarrow \text{FindMaxRadius}(\mathbf{q}_{\text{rand}})$ ;
7:    $\mathbf{x}_{\text{rand}} \leftarrow (\mathbf{q}_{\text{rand}}, r_{\text{rand}})$ ;
8:    $\mathbf{x}_{\text{nearest}} \leftarrow \text{Nearest}(\mathbf{q}_{\text{rand}}, \mathcal{G})$ ;
9:    $\mathbf{x}_{\text{new}} \leftarrow \text{TubeSteer}(\mathbf{x}_{\text{nearest}}, \mathbf{x}_{\text{rand}})$ ;
10:  if  $r_{\text{new}} > r_{\text{min}}$  then
11:     $X_{\text{near}} \leftarrow \text{NearConnect}(\mathcal{G}, \mathbf{x}_{\text{new}})$ ;
12:     $V \leftarrow V \cup \{\mathbf{x}_{\text{new}}\}$ ;
13:     $E \leftarrow \text{Rewire}(\mathbf{x}_{\text{new}}, X_{\text{near}}, E)$ ;
14:  end if
15: end for
16: return  $\mathcal{G} = (V, E)$ ;

```

---

than the maximum radius  $r_{\text{max}}$  defined based on environment and swarm conditions.

**TubeSteer:** The sphere  $\mathbf{x}_{\text{rand}}$  centered at  $\mathbf{q}_{\text{rand}}$  may not have intersections with the sphere  $\mathbf{x}_{\text{nearest}}$  centered at  $\mathbf{q}_{\text{nearest}}$ , as shown in Fig. 2(b). Thus, the sphere  $\mathbf{x}_{\text{rand}}$  needs to be moved to the sphere  $\mathbf{x}_{\text{new}}$  to have an intersection between  $\mathbf{x}_{\text{new}}$  and  $\mathbf{x}_{\text{nearest}}$ , as shown in Fig. 2(c). The details of the function TubeSteer is depicted in *Algorithm 2*.

---

#### Algorithm 2 TubeSteer

---

**Input:** sample sphere  $\mathbf{x}_{\text{rand}}$ , nearest sphere  $\mathbf{x}_{\text{nearest}}$

**Output:** updated sphere  $\mathbf{x}_{\text{new}}$

```

1:  $(\mathbf{q}_{\text{new}}, r_{\text{new}}) \leftarrow \mathbf{x}_{\text{rand}}$ ;  $(\mathbf{q}_{\text{nearest}}, r_{\text{nearest}}) \leftarrow \mathbf{x}_{\text{nearest}}$ ;
2:  $d \leftarrow \|\mathbf{q}_{\text{new}} - \mathbf{q}_{\text{nearest}}\|$ ;
3:  $\mathbf{t} \leftarrow (\mathbf{q}_{\text{new}} - \mathbf{q}_{\text{nearest}}) / \|\mathbf{q}_{\text{new}} - \mathbf{q}_{\text{nearest}}\|$ ;
4: while  $r_{\text{new}}$  and  $r_{\text{nearest}}$  is less than  $d$  do
5:    $d \leftarrow \max(r_{\text{new}}, r_{\text{nearest}})$ ;
6:    $\mathbf{q}_{\text{new}} \leftarrow \mathbf{q}_{\text{nearest}} + d \cdot \mathbf{t}$ ;
7:    $r_{\text{new}} \leftarrow \text{FindMaxRadius}(\mathbf{q}_{\text{new}})$ ;
8: end while
9: return  $\mathbf{x}_{\text{new}} \leftarrow (\mathbf{q}_{\text{new}}, r_{\text{new}})$ ;

```

---

**NearConnect:** Find a set of the spheres, denoted by  $X_{\text{near}}$ ,

in which all spheres have intersections with the new sphere  $\mathbf{x}_{\text{new}}$ . The details are described in *Algorithm 3*.

**Rewire:** Rewire the new sphere  $\mathbf{x}_{\text{new}}$  to the near sphere which has the minimum cost in  $X_{\text{near}}$ . And all spheres in  $X_{\text{near}}$  also are rewired, as shown in *Algorithm 4*.

---

### Algorithm 3 NearConnect

---

**Input:** tree  $\mathcal{G}$ , new sphere  $\mathbf{x}_{\text{new}}$   
**Output:** a set of near spheres  $X_{\text{near}}$

- 1:  $(V, E) \leftarrow \mathcal{G}$ ,  $(\mathbf{q}_{\text{new}}, r_{\text{new}}) \leftarrow \mathbf{x}_{\text{new}}$ ;
- 2:  $X_{\text{near}} \leftarrow \emptyset$ ;
- 3: **for**  $\mathbf{x}_{\text{near}} \in V$  **do**
- 4:    $(\mathbf{q}_{\text{near}}, r_{\text{near}}) \leftarrow \mathbf{x}_{\text{near}}$ ;
- 5:    $d \leftarrow \|\mathbf{q}_{\text{new}} - \mathbf{q}_{\text{near}}\|$ ;
- 6:   **if**  $r_{\text{near}} + r_{\text{new}} > d$  **then**
- 7:      $X_{\text{near}} \leftarrow X_{\text{near}} \cup \mathbf{x}_{\text{near}}$ ;
- 8:   **end if**
- 9: **end for**
- 10: **return**  $X_{\text{near}}$ ;

---

**Score:** A Score function is designed to score a connection between two adjacent spheres, considering both the distance and the volume of sphere-sphere intersections, as depicted in

$$\text{Score} = \rho_d \frac{\|\mathbf{q}_{\text{new}} - \mathbf{q}_{\text{near}}\|}{\|\mathbf{q}_{\text{goal}} - \mathbf{q}_{\text{init}}\|} + \rho_v \left( \frac{V_{\text{int}}}{\sigma_v} + \varepsilon \right)^{-1}, \quad (3)$$

where  $\rho_v$  and  $\rho_d$  are weight coefficients,  $V_{\text{int}}$  is the volume of the intersection between spheres of  $\mathbf{q}_{\text{new}}$  and  $\mathbf{q}_{\text{near}}$ , and  $\sigma_v, \varepsilon$  are constants.

---

### Algorithm 4 Rewire

---

**Input:** edges  $E$ , new sphere  $\mathbf{x}_{\text{new}}$ , a set of near spheres  $X_{\text{near}}$   
**Output:** edges  $E$

- 1:  $\mathbf{x}_{\text{min}} \leftarrow \mathbf{x}_{\text{nearest}} \in X_{\text{near}}$ ;
- $c_{\text{min}} \leftarrow \text{Cost}(\mathbf{x}_{\text{nearest}}) + \text{Score}(\mathbf{x}_{\text{nearest}}, \mathbf{x}_{\text{new}})$ ;
- 2: **for**  $\mathbf{x}_{\text{near}} \in X_{\text{near}}$  **do**
- 3:   **if**  $\text{ObstacleFree}(\mathbf{x}_{\text{near}}, \mathbf{x}_{\text{new}}) \wedge \text{Cost}(\mathbf{x}_{\text{near}}) + \text{Score}(\mathbf{x}_{\text{near}}, \mathbf{x}_{\text{new}}) < c_{\text{min}}$  **then**
- 4:      $\mathbf{x}_{\text{min}} \leftarrow \mathbf{x}_{\text{near}}$ ;
- $c_{\text{min}} \leftarrow \text{Cost}(\mathbf{x}_{\text{near}}) + \text{Score}(\mathbf{x}_{\text{near}}, \mathbf{x}_{\text{new}})$ ;
- 5:   **end if**
- 6: **end for**
- 7:  $E \leftarrow E \cup \{(\mathbf{x}_{\text{min}}, \mathbf{x}_{\text{new}})\}$ ;
- 8: **for**  $\mathbf{x}_{\text{near}} \in X_{\text{near}}$  **do**
- 9:   **if**  $\text{ObstacleFree}(\mathbf{x}_{\text{near}}, \mathbf{x}_{\text{new}}) \wedge \text{Cost}(\mathbf{x}_{\text{new}}) + \text{Score}(\mathbf{x}_{\text{near}}, \mathbf{x}_{\text{new}}) < \text{Cost}(\mathbf{x}_{\text{near}})$  **then**
- 10:      $\mathbf{x}_{\text{parent}} \leftarrow \text{Parent}(\mathbf{x}_{\text{near}})$ ;
- $E \leftarrow (E \setminus \{(\mathbf{x}_{\text{parent}}, \mathbf{x}_{\text{near}})\}) \cup \{(\mathbf{x}_{\text{new}}, \mathbf{x}_{\text{near}})\}$ ;
- 11:   **end if**
- 12: **end for**
- 13: **return**  $E$ ;

---

The Tube-RRT\* algorithm, as depicted in *Algorithm 1*, incorporates the addition of a new sphere to the vertex set  $V$  while considering both distance and volume of intersection.

Consequently, only spheres that intersect with a sphere from the tree are added as new node, ensuring that any tree node has intersections with adjacent nodes. During the selection of the parent node and tree rewiring process, the score defined in (3) accounts for both distance and volume of intersection between adjacent spheres. This implies that the new sphere tends to select a parent node with a shorter distance and larger intersection volume, resulting in paths generated by the Tube-RRT\* algorithm having shorter lengths within a broader space.

### C. Homotopic Paths Generation

The generation method of the homotopic paths based on Tube-RRT\* is described in this section. In the optimal virtual tube planning method [6], the boundary optimal trajectories of the virtual tube based on the boundary paths are generated first. Then, the trajectory within the virtual tube is optimal when the coefficients of the trajectory are the interpolation among coefficients of the boundary trajectories, which implies that the path points of the trajectory within the virtual tube are the interpolation of the boundary path points. Thus, the homotopic path can be generated by the interpolation among boundary paths. The homotopic path  $\sigma_\theta$  within the virtual tube can be expressed as

$$\begin{aligned} \sigma_\theta &= \sigma \left( \left( \sum_{k=1}^M \theta_k \mathbf{q}_{0,k}, \sum_{k=1}^M \theta_k \mathbf{q}_{m,k} \right), t \right) \\ &= \sum_{k=1}^M \theta_k \sigma((\mathbf{q}_{0,k}, \mathbf{q}_{m,k}), t) = \sum_{k=1}^M \theta_k \sigma_k, \end{aligned} \quad (4)$$

where  $\sum_{k=1}^M \theta_k = 1, \theta_k \geq 0$ ,  $\mathbf{q}_{0,k}$  and  $\mathbf{q}_{m,k}$  are vertexes of the terminal  $\mathcal{C}_0$  and  $\mathcal{C}_1$  respectively,  $M$  is the number of the vertexes in terminals,  $\sigma_k$  are the boundary paths. Combining (4) with the process in *Algorithm 1*, the time complexity of homotopic paths generation is  $O(n(\log n + 1) + 1)$  where  $n$  is the number of samples. Compared with the time complexity  $O(n(\log n + 1))$  of RRT\* [15], the time complexity of paths interpolated by the boundary path points is independent of the number of samples  $n$ .

Thus, the key of homotopic paths generation is to generate the boundary paths. For the boundary paths  $\sigma_k$ , terminal path points  $\mathbf{q}_{0,k}$  and  $\mathbf{q}_{m,k}$  in  $\sigma_k$ , as shown in Fig. 3(a), are vertexes of terminals  $\mathcal{C}_0$  and  $\mathcal{C}_1$ , and intermediate path points  $\mathbf{q}_{i,k}$  are selected in the spherical intersections between adjacent spheres centered at  $\mathbf{q}_{i-1}$  and  $\mathbf{q}_i$ , as shown in Fig. 3(b). The spherical intersection  $\mathcal{I}_i$  of adjacent spheres centered in  $\mathbf{q}_{i-1}$  and  $\mathbf{q}_i$  is expressed as

$$\mathcal{I}_i(\rho, \theta) = \mathbf{q}_{o,i} + \rho \lambda_i (\mathbf{n}_{o,i} \cos \theta + \mathbf{b}_{o,i} \sin \theta), \quad (5)$$

where  $\theta \in [0, 2\pi]$ ,  $\rho \in [0, 1]$ ,  $\mathbf{n}_{o,i}$  and  $\mathbf{b}_{o,i}$  are unit normal vector and unit abnormal vector of the line  $\overline{\mathbf{q}_i \mathbf{q}_{i-1}}$  respectively,

$$\begin{aligned} \mathbf{q}_{o,i} &= \mathbf{q}_{i-1} + \frac{r_{i+1}^2 - r_i^2 + \|\mathbf{q}_i - \mathbf{q}_{i-1}\|^2}{2 \|\mathbf{q}_i - \mathbf{q}_{i-1}\|} \mathbf{v}_{o,i}, \\ \lambda_i &= \sqrt{r_{i+1}^2 - \frac{r_{i+1}^2 - r_i^2 + \|\mathbf{q}_{i+1} - \mathbf{q}_i\|^2}{2 \|\mathbf{q}_{i+1} - \mathbf{q}_i\|}}, \end{aligned}$$

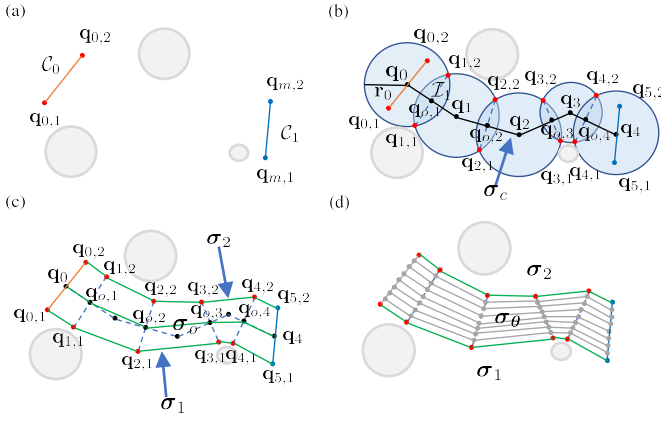


Fig. 3. Examples of homotopic paths generation. (a) Red line and blue line represent terminal  $C_0$  and  $C_1$  respectively. (b) Tube-RRT\* algorithm generates a path  $\sigma_c$  from  $q_0$  to  $q_4$  represented by the black line. (c) Boundary paths denoted by green lines. (d) Homotopic paths  $\sigma_\theta$  are represented by the gray lines.

$\mathbf{v}_{o,i}$  is the unit tangent vector.

Let the path  $\sigma_o$  be a sequence of points  $\{q_{o,i}\}$  ( $i = 0, 1, \dots, m$ ), as shown in Fig. 3(c), where  $q_{o,0} = q_0$  and  $q_{o,m} = q_{m-1}$ . Based on the geometric relationships between  $q_{o,i}$  and  $q_i$  in Fig. 3(b), the path  $\sigma_o$  can be generated by the path  $\sigma_c$  which is a sequence of centers  $q_i$  of spheres with radii  $r_i$  ( $i = 0, 1, \dots, m-1$ ), as shown in Fig. 3(b).

Thus, Tube-RRT\* algorithm first generates the path  $\sigma_c$ . Then, the path  $\sigma_o$  is generated by the path  $\sigma_c$ . The boundary paths and homotopic paths are generated based on the  $\sigma_o$  finally. Here is an example of homotopic paths generation in Fig. 3(a), where the start and goal areas are denoted as terminal  $C_0$  and  $C_1$ , respectively. The vertices of these terminals are  $q_{0,1}$ ,  $q_{0,2}$ ,  $q_{m,1}$ , and  $q_{m,2}$ . Subsequently, the Tube-RRT\* algorithm generates  $\sigma_c$  which is a sequence of intersected spheres  $\{q_i\}$  with radii  $r_i$  ( $i = 0, 1, 2, 3, 4$ ), as illustrated in Fig. 3(b). Then, the path  $\sigma_o = \{q_{o,i}\}$  ( $i = 0, 1, \dots, 5$ ) is generated by  $\sigma_c$ , where  $q_{o,0} = q_0$ , and  $q_{o,5} = q_4$ . The boundary paths  $\sigma_1$  and  $\sigma_2$  are then formed by connecting the boundary points in the spherical intersection, depicted in Fig. 3(c). Finally, the homotopic path  $\sigma_\theta$  is generated by interpolating between the boundary paths  $\sigma_1$  and  $\sigma_2$ , as shown in Fig. 3(d).

#### D. Analysis

In this section, some properties of the proposed algorithm are analyzed. Let  $\sigma_c = \{q_i\}$  ( $i = 0, 1, \dots, m-1$ ) be a collision-free path from start sphere  $\mathbf{x}_{init} = (q_{init}, r_{init})$  to goal sphere  $\mathbf{x}_{goal} = (q_{goal}, r_{goal})$ . The cost of the path  $\sigma_c$  is expressed as

$$\text{Cost}(\sigma_c) = \frac{\rho_d}{\|q_{goal} - q_{init}\|} \sum_{i=1}^{m-1} d_i + \rho_v \sum_{i=1}^{m-1} \left( \frac{V_{int,i}}{\sigma_v} + \epsilon \right)^{-1}, \quad (6)$$

where  $d_i = \|q_i - q_{i-1}\|$  is the distance between centers of adjacent spheres,  $V_{int,i}$  is the intersection volume of the adjacent spheres. The cost of goal point could be regarded as

the a function  $f = f_1 + f_2$  with respect to the number of the segments of the path, the total distance of the path, and the total volume of intersection of spheres, which is expressed as

$$f = \text{Cost}(\sigma_c). \quad (7)$$

And rewiring function implies that the proposed algorithm intends to find a path  $\sigma^*$  with a minimum cost in (7), namely a shorter and more volume path.

The proposed Tube-RRT\* algorithm considers both path length and intersection volume. On the one hand, with the same start and goal points, suppose that two paths with the same path length have been found. A path with more intersection volume would be selected as the desired path. On the other hand, with the same intersection volume, a path with a less path length would be selected as the desired path. Furthermore, with the same length and intersection volume, a path with a smaller number of segments and more average volume of each intersection would be selected as the desired path, which is shown below.

It should be noted that the tube path length in *Definition 5* is represent by  $L(\sigma_o)$ . However, the path length considered in cost (6) is for the path  $L(\sigma_c)$ . Thus, the following *Lemma 1* shows that the length of  $\sigma_o$  can be approximated by the length of path  $\sigma_c$ , if the number of samples tends towards infinity.

*Lemma 1:* For any  $\epsilon > 0$ , there exists  $m_c \in \mathbb{Z}^+$  so that when the number of path points  $m > m_c$  for the path  $\sigma_o$ ,  $L(\sigma_c) - L(\sigma_o) \leq \epsilon$ .

*Proof:* See details in *Appendix A*.  $\blacksquare$

Based on *Lemma 1*, the length  $\sigma_c$  could be used in (7) to minimizing the tube path length. Then, a proposition is obtained to show a property which is beneficial for the virtual tube as the following:

*Proposition 1:* Let  $\Sigma_\sigma$  be a set of feasible paths, where  $m_{min}$  denotes the minimum number of path points in  $\Sigma_\sigma$ . Suppose all paths in  $\Sigma_\sigma$  have equal tube path lengths and equal total volume  $V_{total}$ . Then, the path  $\sigma^*$  with the minimum cost in  $\Sigma_\sigma$  is found when the number of path points for  $\sigma^*$  is  $m_{min}$ , and the intersection volumes  $V_{int,i}$  between any adjacent path points are  $V_{total}/m_{min}$ .

*Proof:* See details in *Appendix B*.  $\blacksquare$

## IV. SIMULATIONS

In this section, we initially outline the setup details for the simulations. Subsequently, we conduct comparisons between the proposed tube path planning algorithm with volume consideration *enabled* and *disabled*, namely  $\rho_v > 0$  and  $\rho_v = 0$  in (6) respectively, across various metrics to validate the performance of our algorithm.

### A. Simulation Setup

The proposed algorithm in MATLAB code is implemented on a PC with Intel Core i7-13900KF@ 3.0 GHz CPU and 32G RAM. A map with random obstacles is used for tube path planning. The size of the map used for simulation is  $250 \times 200 \times 30$ m, and the parameters for the path planning algorithm are set as follows:  $\rho_d = 1$ ,  $\sigma_v = 1413.7$ , and  $\epsilon =$

0.01. The  $\rho_v$  is set as 0 for disabled volume consideration and 0.15 for enabled volume consideration. The start and goal areas are consistent across all tests. The swarm consists of 20 drones, with a safety radius of 0.5m and an avoidance radius of 1m. The maximum speed is set to 7m/s.

### B. Tube Path Planning Results

This subsection compares between the Tube-RRT\* algorithms with volume consideration *enabled* and *disabled* in maps with varying numbers of random obstacles. For simply, the Tube-RRT\* algorithms with volume consideration *enabled* and *disabled* are denoted as Tube-RRT\* and disabled Tube-RRT\* respectively. It examines the differences between them in terms of average tube length, minimum sphere volume, and computation time. These three metrics are described in the following.

- Average tube length (ATL): The tube path length is determined by connecting the centers of the spheres generated by the path planning algorithm. The average tube length is computed by taking the average of all the lengths of tube paths in the tests.
- Minimum sphere volume (MSV): The volume of the smallest sphere among the spheres generated by the path planning algorithm, representing the volume of the smallest gap through which the tube passes.
- Computation time (CT): The time required for the computer to generate tube paths.

Multiple simulation tests have been performed on the path planning algorithms in different obstacle environments, as shown in Fig. 4. In scenarios with the same number of obstacles, the positions of the obstacles are randomized for each test. The statistical metrics are presented in Table I and Fig. 5.

From Table I, it can be observed that the Tube-RRT\* algorithm has a relatively larger minimum gap volume and a longer average tube length compared to the disabled Tube-RRT\* algorithm, with little difference in computation time. When the number of obstacles is small, the three metrics for both algorithms exhibit little difference. Meanwhile, as shown in Fig. 4(a), the generated paths appear to be quite similar. As the number of obstacles increases, the ATL of Tube-RRT\* increases significantly and the MSV of Tube-RRT\* is larger than that of disabled Tube-RRT\*. These differences can also be observed in Fig. 4(b). This suggests that the Tube-RRT\* algorithm strikes a balance between tube length and gap volume, sacrificing the shortest path in exchange for larger gap spaces. Such a choice proves advantageous for the swarm of drones navigating the virtual tube, as it helps to avoid congestion at narrow passages, thereby enhancing traversal efficiency.

However, in scenarios where the number of obstacles is excessively high, Tube-RRT\* tends to converge towards the disabled RRT\* algorithm in terms of minimum gap volume, as illustrated in Fig. 5(b). Consequently, the Tube-RRT\* algorithm demonstrates more pronounced performance in large-scale, obstacle-dense environments.

Number of obstacles	Metrics	Methods	
		Disabled	Enabled
20	ATL (m)	<b>226.31</b>	245.73
	MSV (m <sup>3</sup> )	2990.22	<b>8174.12</b>
	CT (s)	12.29	<b>12.14</b>
30	ATL (m)	<b>237.69</b>	270.11
	MSV (m <sup>3</sup> )	1084.25	<b>4749.39</b>
	CT (s)	<b>11.34</b>	11.37
40	ATL (m)	<b>242.92</b>	287.82
	MSV (m <sup>3</sup> )	1017.25	<b>3232.28</b>
	CT (s)	10.91	<b>10.85</b>
50	ATL (m)	<b>255.13</b>	306.19
	MSV (m <sup>3</sup> )	839.48	<b>2006.56</b>
	CT (s)	<b>10.90</b>	11.03
60	ATL (m)	83.3	<b>65.3</b>
	MSV (m <sup>3</sup> )	398.45	<b>2034.38</b>
	CT (s)	<b>4.6201</b>	4.8541
70	ATL (m)	<b>267.90</b>	316.69
	MSV (m <sup>3</sup> )	338.63	<b>562.87</b>
	CT (s)	<b>10.10</b>	10.16

TABLE I  
PERFORMANCE METRICS FOR DIFFERENT METHODS IN COMPLEX SCENARIOS WITH A VARIED NUMBER OF OBSTACLES.

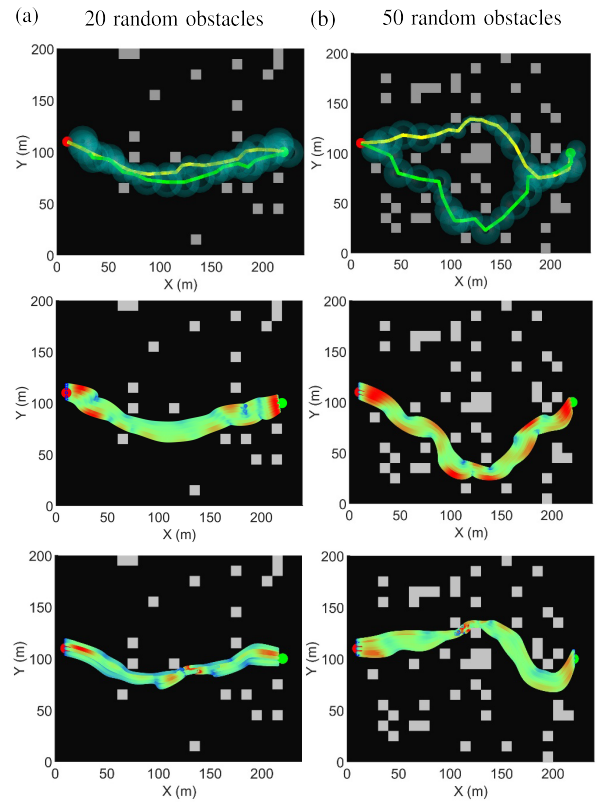


Fig. 4. Comparisons between path planning algorithms for virtual tubes. The red and green points represent the start area and goal area respectively. And the green curves and yellow curves are generated by Tube-RRT\* and disabled Tube-RRT\* respectively. The colorful curves represent trajectories for robots and the colors from blue to red represent the speed from zero to maximum.

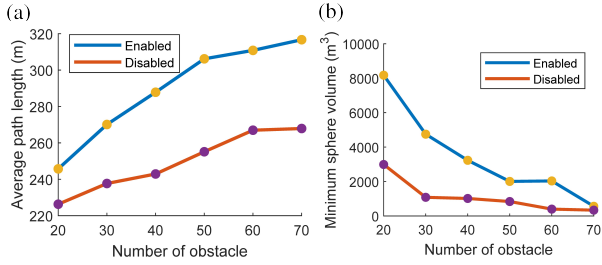


Fig. 5. Metrics of paths with varying numbers of obstacles.

Obstacles	20	30	40	50	60
Disabled	90.1s	93.4s	96.8s	91.3s	92.8s
Enabled	90.1s	89.0s	89.5s	89.0s	88.9s

TABLE II

FLIGHT TIMES OF TWO METHODS IN MAPS WITH VARIOUS OBSTACLES.

### C. Simulate Flight Results

In this subsection, optimal virtual tubes are generated based on the homotopic paths planned in the previous subsection. The distributed swarm controller and planning method remain consistent with those described in [6]. The desired flight time is standardized to 90s across all scenarios. Through the comprehensive comparisons of various metrics, including flight time, flight speed, and minimum distance among drones, the effectiveness of the proposed method is validated.

When the obstacles in the environment are relatively sparse, the tube paths planned by the two algorithms show minimal differences, resulting in similar flight times, as shown in Table II. However, in obstacle-dense environments, as shown in Fig. 4(b), the flight results diverge significantly. Specifically, in terms of flight time, as detailed in Table II, the Tube-RRT\* algorithm yields the result allowing the swarm to reach the target area in a shorter time. Conversely, the virtual tube generated by the disabled Tube-RRT\* algorithm navigates through narrow passages, leading to congestion within the swarm. This congestion is evident in the blue area in Fig. 6(a), where the flight speed of the swarm experiences more drastic fluctuations compared with the virtual tube generated by Tube-RRT\* shown in Fig. 6(b), resulting in increased collision risk and reduced safety. In addition, as shown in Fig. 7, the proximity of the drone exceeds the safe distance threshold when traversing narrow gaps.

## V. CONCLUSION

The Tube-RRT\* algorithm is introduced for planning homotopic paths within optimal virtual tubes, distinguished by its simultaneous consideration of the gap volume and the path length. This facilitates the selection of larger spaces within obstacle environments by the optimal virtual tube. Through comparative simulations, our proposed approach has been substantiated to significantly improve the capability of swarm to navigate obstacle environments swiftly. Future endeavors will explore the generation of multiple non-homotopic paths to facilitate virtual tube network planning.

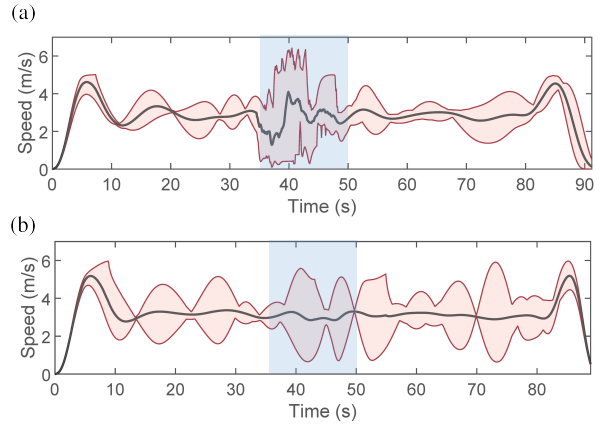


Fig. 6. Swarm speed distributions over time in a map with 50 random obstacles. The red curves and black curves represent the maximum speed, minimum speed, and average speed of the swarm. (a) Speed distributions in the tube based on the disabled Tube-RRT\* algorithm. The blue block represents the segment of passing through narrow gaps in the tube based on the Tube-RRT\* algorithm.

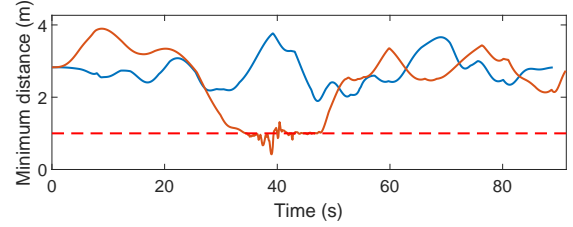


Fig. 7. The minimum distances among drones in a map with 50 obstacles. The red curve and blue curve represent the minimum distance in tubes generated by disabled Tube-RRT\* and Tube-RRT\* respectively. And, the red line represents the safety distance among drones.

## REFERENCES

- [1] X. Zhou, X. Wen, Z. Wang, Y. Gao, H. Li, Q. Wang, T. Yang, H. Lu, Y. Cao, C. Xu, *et al.*, "Swarm of Micro Flying Robots in the Wild," *Science Robotics*, vol. 7, no. 66, 2022.
- [2] G. Vásárhelyi, C. Virágh, G. Somorjai, T. Nepusz, A. E. Eiben, and T. Vicsek, "Optimized Flocking of Autonomous Drones in Confined Environments," *Science Robotics*, vol. 3, no. 20, 2018.
- [3] Q. Quan, Y. Gao, and C. Bai, "Distributed Control for a Robotic Swarm to Pass Through a Curve Virtual Tube," *Robotics and Autonomous Systems*, vol. 162, 2023.
- [4] V. Usenko, L. von Stumberg, A. Pangercic, and D. Cremers, "Real-time Trajectory Replanning for MAVs using Uniform B-splines and A 3D Circular Buffer," in *2017 IEEE/RSJ International Conference on Intelligent Robots and Systems (IROS)*. IEEE, 2017, pp. 215–222.
- [5] W. Ding, W. Gao, K. Wang, and S. Shen, "An Efficient B-Spline-Based Kinodynamic Replanning Framework for Quadrotors," *IEEE Transactions on Robotics*, vol. 35, no. 6, pp. 1287–1306, 2019.
- [6] P. Mao, R. Fu, and Q. Quan, "Optimal Virtual Tube Planning and Control for Swarm Robotics," *The International Journal of Robotics Research*, vol. 43, no. 5, pp. 602–627, 2024.
- [7] T. Osa, "Motion Planning by Learning the Solution Manifold in Trajectory Optimization," *The International Journal of Robotics Research*, vol. 41, no. 3, pp. 281–311, 2022.
- [8] M. Likhachev, G. J. Gordon, and S. Thrun, "ARA\*: Anytime A\* with Provable Bounds on Sub-optimality," *Advances in Neural Information Processing Systems*, vol. 16, 2003.
- [9] S. M. LaValle and J. J. Kuffner Jr, "Randomized Kinodynamic Planning," *The International Journal of Robotics Research*, vol. 20, no. 5, pp. 378–400, 2001.
- [10] E. W. Dijkstra, "A Note on Two Problems in Connexion with Graphs," in *Edsger Wybe Dijkstra: His Life, Work, and Legacy*, 2022, pp. 287–290.

- [11] F. Xie, M. Müller, and R. Holte, "Jasper: the Art of Exploration in Greedy Best First Search," *The Eighth International Planning Competition (IPC-2014)*, pp. 39–42, 2014.
- [12] P. E. Hart, N. J. Nilsson, and B. Raphael, "A Formal Basis for the Heuristic Determination of Minimum Cost Paths," *IEEE Transactions on Systems Science and Cybernetics*, vol. 4, no. 2, pp. 100–107, 1968.
- [13] L. E. Kavraki, P. Svestka, J.-C. Latombe, and M. H. Overmars, "Probabilistic Roadmaps for Path Planning in High-dimensional Configuration Spaces," *IEEE Transactions on Robotics and Automation*, vol. 12, no. 4, pp. 566–580, 1996.
- [14] S. M. LaValle, "Rapidly-exploring Random Trees: A New Tool for Path Planning," *The Annual Research Report*, 1998.
- [15] S. Karaman and E. Frazzoli, "Sampling-based Algorithms for Optimal Motion Planning," *The International Journal of Robotics Research*, vol. 30, no. 7, pp. 846–894, 2011.
- [16] C. Moon and W. Chung, "Kinodynamic Planner Dual-tree RRT (DT-RRT) for Two-wheeled Mobile Robots using the Rapidly Exploring Random Tree," *IEEE Transactions on Industrial Electronics*, vol. 62, no. 2, pp. 1080–1090, 2014.
- [17] O. Salzman and D. Halperin, "Asymptotically Near-optimal RRT for Fast, High-quality Motion Planning," *IEEE Transactions on Robotics*, vol. 32, no. 3, pp. 473–483, 2016.
- [18] W. Zhang, L. Shan, L. Chang, and Y. Dai, "SVF-RRT\*: A Stream-Based VF-RRT\* for USVs Path Planning Considering Ocean Currents," *IEEE Robotics and Automation Letters*, vol. 8, no. 4, pp. 2413–2420, 2023.
- [19] J. R. Munkres, *Topology*. Pearson, 2014.
- [20] E. Hernandez, M. Carreras, and P. Ridao, "A Comparison of Homotopic Path Planning Algorithms for Robotic Applications," *Robotics and Autonomous Systems*, vol. 64, pp. 44–58, 2015.
- [21] J. Kim and J. P. Ostrowski, "Motion Planning a Aerial Robot Using Rapidly-Exploring Random Trees with Dynamic Constraints," in *2003 IEEE International Conference on Robotics and Automation (ICRA)*, vol. 2. IEEE, 2003, pp. 2200–2205.
- [22] D. Yi, M. A. Goodrich, and K. D. Seppi, "Homotopy-Aware RRT\*: Toward Human-Robot Topological Path-Planning," in *2016 11th ACM/IEEE International Conference on Human-Robot Interaction (HRI)*. IEEE, 2016, pp. 279–286.
- [23] J. Liu, M. Fu, A. Liu, W. Zhang, and B. Chen, "A Homotopy Invariant Based on Convex Dissection Topology and a Distance Optimal Path Planning Algorithm," *IEEE Robotics and Automation Letters*, vol. 8, no. 11, pp. 7695–7702, 2023.
- [24] J. Fu, W. Yao, G. Sun, H. Tian, and L. Wu, "An FTSA Trajectory Elliptical Homotopy for Unmanned Vehicles Path Planning with Multi-Objective Constraints," *IEEE Transactions on Intelligent Vehicles*, vol. 8, no. 3, pp. 2415–2425, 2023.
- [25] F. M. Dekking, *A Modern Introduction to Probability and Statistics: Understanding Why and How*. Springer Science & Business Media, 2005.

## APPENDIX

### A. The Proof of Lemma 1

The length of  $\sigma_c$  is expressed as

$$\begin{aligned} L(\sigma_c) &= \sum_{i=1}^{m-1} \|\mathbf{q}_i - \mathbf{q}_{i-1}\| \\ &= \sum_{i=1}^{m-1} (\|\mathbf{q}_i - \mathbf{q}_{o,i}\| + \|\mathbf{q}_{o,i} - \mathbf{q}_{i-1}\|). \end{aligned} \quad (8)$$

And the length of  $\sigma_o$  is expressed as

$$L(\sigma_o) = \sum_{i=1}^m \|\mathbf{q}_{o,i} - \mathbf{q}_{o,i-1}\|, \mathbf{q}_{o,0} = \mathbf{q}_0, \mathbf{q}_{o,m} = \mathbf{q}_{m-1}. \quad (9)$$

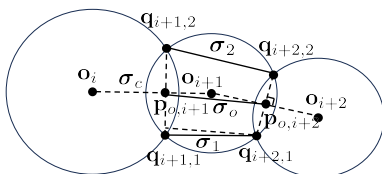


Fig. 8. The relationships among different paths.

Combining the triangle inequality

$$\|\mathbf{q}_{o,i} - \mathbf{q}_{o,i-1}\| \leq \|\mathbf{q}_i - \mathbf{q}_{o,i}\| + \|\mathbf{q}_{i-1} - \mathbf{q}_{o,i}\| \quad (10)$$

with the uniform random sampling, for any  $\epsilon > 0$ , there exists  $m_c \in \mathbb{Z}^+$  such that when  $m > m_c$ ,

$$\max \{\|\mathbf{q}_i - \mathbf{q}_{o,i}\|\} \leq \frac{\epsilon}{m}. \quad (11)$$

Thus, combining (8), (9), (10) with (11), we can obtain that

$$L(\sigma_c) - L(\sigma_o) \leq \epsilon. \quad (12)$$

### B. The Proof of Proposition 1

Let  $V_{\text{total}}$  be the total intersection volume of the path. The problem which satisfies KKT condition can be expressed as a convex optimization problem

$$\min_{V_{\text{int},i}, m} \sum_{i=1}^{m-1} (V_{\text{int},i}/\sigma_v + \epsilon)^{-1} \quad (13a)$$

$$\text{s.t.} \sum_{i=1}^n V_{\text{int},i} = V_{\text{total}}, \quad (13b)$$

$$V_{\text{int},i} > 0, i = 1, \dots, m-1, \quad (13c)$$

$$m \geq m_{\min} \in \mathbb{Z}^+. \quad (13d)$$

A step-by-step approach to optimization is used. First, variables  $V_{\text{int},i}$  are optimized. Then, optimal  $m$  is obtained.

The Lagrange function of problem (13) is obtained by

$$\begin{aligned} L(V_{\text{int},i}, \lambda, \mu_i) &= \sum_{i=1}^{m-1} (V_{\text{int},i}/\sigma_v + \epsilon)^{-1} + \\ &\lambda \left( \sum_{i=1}^{m-1} V_{\text{int},i} - V_{\text{total}} \right) - \sum_{i=1}^{m-1} \mu_i V_{\text{int},i}. \end{aligned} \quad (14)$$

Thus, KKT condition contains

$$\nabla_{V_{\text{int},i}} L = -\sigma_v^{-1} (V_{\text{int},i}/\sigma_v + \epsilon)^{-2} + \lambda - \mu_i = 0, \quad (15a)$$

$$\sum_{i=1}^{m-1} V_{\text{int},i} - V_{\text{total}} = 0, \quad (15b)$$

$$-V_{\text{int},i} \leq 0, \quad (15c)$$

$$\mu_i \geq 0, \quad (15d)$$

$$\mu_i V_{\text{int},i} = 0, i = 1, \dots, m-1. \quad (15e)$$

Combining (13c), (15d) and (15e), we could obtain that  $\mu_i = 0$ , so that (15a) can be expressed as

$$\lambda = \sigma_v^{-1} (V_{\text{int},i}/\sigma_v + \epsilon)^{-2}, i = 1, \dots, m-1. \quad (16)$$

Substitute (16) into (15b) to obtain that

$$V_{\text{int},i}^* = V_{\text{total}}/n, i = 1, \dots, m-1. \quad (17)$$

In the next step, substitute (17) into (13) to obtain a new optimization problem which is expressed as

$$\min_{m \in \mathbb{Z}^+} \frac{(m-1)^2}{\frac{V_{\text{total}}}{\sigma_v} + \epsilon(m-1)} \quad (18a)$$

$$\text{s.t. } m \geq m_{\min}. \quad (18b)$$

The objective function in (18a) is monotonically decreasing with respect to  $m$ . Thus, the solution to (18) is  $m_{\min}$ , namely, the minimum number of path points.